

Analytical Solution to Scattering of N Plane Waves by a Coated Circular Cylinder

MUHAMMAD A MUSHREF
 PO Box 9772, Jeddah 21423
 SAUDI ARABIA

Abstract: – Electromagnetic scattering patterns by a coated circular cylinder are examined for N incident plane waves. Transverse electric (TE) fields are assumed in the problem and expressed as an infinite series. The boundary value method is applied to find the radiations diffracted by the structure. Wave transformation and orthogonality of the complex exponentials are employed to produce an infinite series in the solution. Numerical results are then shown by shortening the infinite series to a limited number of terms.

Key- Words: – Scattering, Plane Waves, Radiation Patterns, Cylindrical Reflector, Boundary Value Analysis.

1 Introduction

Scattering patterns by coated circular cylinders were considered in several researches [1–6]. In [1], theoretical and experimental results for the backscattering from coated cylinders were achieved and the dielectric coating was assumed lossless with a thickness comparable to the wavelength. A low frequency solution was found in [2] to the diffraction of a plane wave incident on a dielectric-loaded trough in a conducting plane. In [3], the eigenvalue solution was also changed into a high frequency ray solution where the scattered fields were expressed in terms of a geometrical optics ray and two surface waves around the cylinder. In addition, a dual-series eigenfunction solution was determined in [4] for scattering by a semicircular channel in a ground plane. The scattered radiations were found in a simple closed-form low-frequency asymptotic approximation. In [5], plane wave scattering at oblique incidence from a circular dielectric cylinder was also solved. The oblique incidence contains a significant cross polarized component which vanishes at normal incidence. TM (transverse magnetic) scattering of two incident plane waves by a dielectric coated cylinder was first investigated in [6]. Various scattering patterns and characteristics were found at different angles of incidence.

In this paper, the TE characteristics are investigated for N incident plane waves on a circular cylinder with a coating substance as shown in Figure 1. The cylinder is assumed to be thin and perfectly conducting with radius a and with infinite extent along the z -axis. The covering layer is taken as region I with radius b and assumed linear, isotropic and homogenous with permeability μ and

permittivity ε . N plane waves are incident on the coated cylinder with different amplitudes and angles of incidence with respect to the x -axis. Free space away from the dielectric material with μ_0 and ε_0 is assumed region II.

2 Theory and Solution

Mathematical formulation starts by solving the Helmholtz scalar wave equation in the circular cylindrical coordinate system in two dimensions r and ϕ [1]. The solution is the cylindrical function which is a Bessel or Hankel function in r multiplied by a complex exponential in ϕ [7,8].

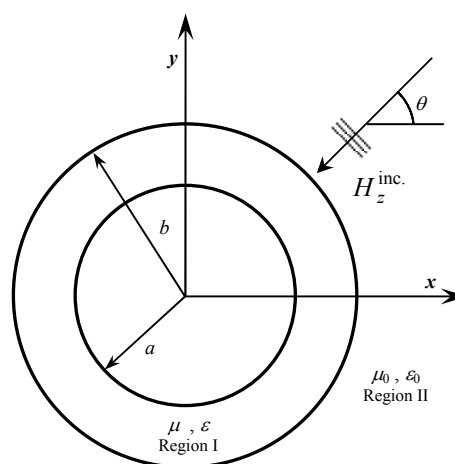


Fig. 1. Geometry of the problem.

As shown in Figure 1, the TE to z incident plane wave as a function of r and ϕ can be expressed in cylindrical coordinates as [1]:

$$H_z^{\text{inc.}}(r, \phi) = H_0 e^{ik_0 r \cos(\phi - \theta)} \quad (1)$$

where H_0 is the wave amplitude, $i = \sqrt{-1}$, k_0 is the free space wave number and θ is the angle of incidence with respect to the x-axis.

The total incident wave is therefore the summation of N incident waves of equation 1. That is:

$$H_z^{\text{inc.tot.}}(r, \phi) = \sum_{L=1}^N H_{0L} e^{ik_0 r \cos(\phi - \theta_L)} \quad (2)$$

By employing the wave transformation method the total incident wave can be expressed in terms of an infinite Fourier-Bessel series as [9,10]:

$$H_z^{\text{inc.tot.}}(r, \phi) = \sum_{n=-\infty}^{\infty} i^n J_n(k_0 r) e^{in\phi} \sum_{L=1}^N H_{0L} e^{-in\theta_L} \quad (3)$$

$$\forall r \geq b \text{ and } 0 \leq \phi \leq 2\pi$$

where $J_n(x)$ is the Bessel function of the first kind with argument x and order n and $n \in I$.

In addition, the diffracted field is defined as an infinite series in region II as [5]:

$$H_z^{\text{diff}}(r, \phi) = \sum_{n=-\infty}^{\infty} A_n e^{in\phi} H_n^{(2)}(k_0 r) \quad (4)$$

$$\forall r \geq b \text{ and } 0 \leq \phi \leq 2\pi$$

where $H_n^{(2)}(x)$ is the outgoing Hankel function of the second kind with argument x and order n and $n \in I$.

The total field in region II is the summation of the incident and the diffracted fields described by equations 3 and 4 respectively. i.e. $H_z^{\text{II}} = H_z^{\text{inc.tot.}} + H_z^{\text{diff}}$. That is:

$$H_z^{\text{II}}(r, \phi) = \sum_{n=-\infty}^{\infty} \left\{ i^n J_n(k_0 r) \sum_{L=1}^N H_{0L} e^{-in\theta_L} + A_n H_n^{(2)}(k_0 r) \right\} e^{in\phi} \quad (5)$$

$$\forall r \geq b \text{ and } 0 \leq \phi \leq 2\pi$$

Similarly, the magnetic field inside the coating material is given by [4]:

$$H_z^{\text{I}}(r, \phi) = \sum_{n=-\infty}^{\infty} B_n e^{in\phi} [J_n(kr) + b_n Y_n(kr)] \quad (6)$$

$$\forall a \leq r \leq b \text{ and } 0 \leq \phi \leq 2\pi$$

where $Y_n(x)$ is the Bessel function of the second type with argument x and order n and $n \in I$. k is the coating material wave number given by $k = 2\pi/\lambda$ and λ is the wavelength. A_n , B_n and b_n are unknown coefficients to be determined by the boundary conditions.

Other magnetic field components H_r and H_ϕ are zeros in both regions I and II since the assumed structure is infinite in the z-axis with $\partial H_z / \partial z = 0$. In addition, the r and ϕ components of the electric field in both regions I and II are found as [8]:

$$E_r(r, \phi) = \frac{-i}{\omega \epsilon r} \frac{\partial H_z}{\partial \phi} \quad (7)$$

$$E_\phi(r, \phi) = \frac{i}{\omega \epsilon} \frac{\partial H_z}{\partial r} \quad (8)$$

where H_z is either H_z^{I} or H_z^{II} as in equations 5 and 6 respectively.

As shown in Figure 1, the tangential electric field vanishes on the surface of the perfectly conducting cylinder. Also, the tangential electric and magnetic fields are continuous at the interface between the coating material and free space. That is respectively,

$$\frac{i}{\omega \epsilon} \frac{\partial H_z^{\text{I}}}{\partial r} = 0 \quad r = a \quad 0 \leq \phi \leq 2\pi \quad (9)$$

$$\frac{1}{\epsilon} \frac{\partial H_z^{\text{I}}}{\partial r} = \frac{1}{\epsilon_0} \frac{\partial H_z^{\text{II}}}{\partial r} \quad r = b \quad 0 \leq \phi \leq 2\pi \quad (10)$$

$$H_z^{\text{I}} = H_z^{\text{II}} \quad r = b \quad 0 \leq \phi \leq 2\pi \quad (11)$$

Orthogonality of the complex exponentials is used for solving equations 9, 10 and 11. From equation 9, the b_n coefficients are found as:

$$b_n = -\frac{J'_n(ka)}{Y'_n(ka)} \quad (12)$$

where the prime notation designates differentiation with respect to the argument.

Equations 10 and 11 are then solved together by elimination and the A_n and B_n coefficients are respectively found as:

$$A_n = R_n M_n \quad (13)$$

$$B_n = V_n M_n \quad (14)$$

where

$$R_n = J'_n(k_0 b) U_n - J_n(k_0 b) \quad (15)$$

$$V_n = \begin{bmatrix} J'_n(k_0 b) H_n^{(2)}(k_0 b) \\ -J_n(k_0 b) H_n^{(2)'}(k_0 b) \end{bmatrix} \left[\frac{k \epsilon_0}{k_0 \epsilon} T_n \right]^{-1} \quad (16)$$

$$M_n = \frac{i^n}{H_n^{(2)}(k_0 b) - H_n^{(2)'}(k_0 b) U_n} \sum_{L=1}^N H_{0L} e^{-in\theta_L} \quad (17)$$

$$U_n = \frac{S_n k_0 \epsilon}{T_n k \epsilon_0} \quad T_n \neq 0 \quad (18)$$

$$S_n = J_n(kb) + b_n Y_n(kb) \quad (19)$$

$$T_n = J'_n(kb) + b_n Y'_n(kb) \quad (20)$$

The magnetic and electric field components in regions I and II expressed by equations 5, 6, 7 and 8 can now be numerically evaluated with the coefficients in equations 12, 13 and 14.

The diffracted magnetic field in equation 4 can be evaluated with the A_n coefficients in equation 13. It can also be calculated at a far point for $r \rightarrow \infty$ by applying the asymptotic approximation of the Hankel function [5] to equation 4. That is:

$$H_z^{\text{diff}}(\phi, r) = D(\phi) e^{-i(k_0 r - \pi/4)} \sqrt{\frac{2}{\pi k_0 r}} \quad (21)$$

$$\forall r \rightarrow \infty \text{ and } 0 \leq \phi \leq 2\pi$$

where $D(\phi)$ is the far diffracted field pattern given by:

$$D(\phi) = \sum_{n=-\infty}^{\infty} i^n A_n e^{in\phi} \quad \forall \quad 0 \leq \phi \leq 2\pi \quad (22)$$

3 Results and Discussions

In this part, several numerical computations are executed graphically to clarify the accuracy of the expressions derived. Due to the convergence of the summation in equation 22 the obtained results are only calculated for $n = -20$ to 20 . The diffracted magnetic field is judged against the single incident plane wave in reference [11].

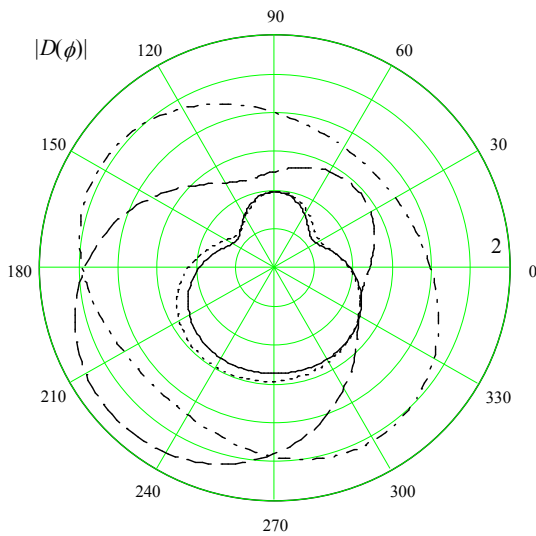


Fig. 2a. Diffracted field patterns for $k_0a = 1$, $\epsilon / \epsilon_0 = 5$, $\mu / \mu_0 = 1$, $H_{01} = 1$ and $\theta_1 = -\pi / 2$. ——— reference [11], $N=2$, $k_0b = 1.01$, $H_{02} = 0.1$, $\theta_2 = \pi$, - - - - $N=2$, $k_0b = 1.1$, $H_{02} = 1$, $\theta_2 = \pi$, - · - · - $N=3$, $k_0b = 1.1$, $H_{02} = H_{03} = 1$, $\theta_2 = \pi$, $\theta_3 = \pi / 4$.

Using equation 22, the diffracted field pattern is displayed in Figure 2a for $N = 2$, $k_0a = 1$, $\epsilon / \epsilon_0 = 5$, $\mu / \mu_0 = 1$, $H_{01} = 1$ and $\theta_1 = -\pi / 2$. The second wave H_{02} is assumed to be very small (0.1) with $\theta_2 = \pi$ and k_0b is considered to be very close to k_0a (1.01) to minimize the effects of the second incident wave and the coating thickness respectively. We can notice good agreements, which confirm the correctness of the expressions derived. Also, in the same Figure the pattern is enhanced and changed when calculated for $N = 2$, $k_0b = 1.1$ and $H_{02} = 1, \theta_2 = \pi$ with a line of symmetry at $\phi = (\theta_1 - \theta_2) / 2 = \pi / 4$ or $-3\pi / 4$. For $N = 3$, $H_{03} = 1, \theta_3 = \pi / 4$ the diffracted pattern is nearly elliptical. Further comparisons are performed in Figure 2b for $N = 2$, $k_0a = 5$, $\epsilon / \epsilon_0 = 5$, $\mu / \mu_0 = 1$, $H_{01} = 1$ and $\theta_1 = -\pi / 2$. Estimations are also taken for $H_{02} = 0.1$ and $k_0b = 5.01$ and we can see good

agreements with reference [11] as well. The pattern is also improved for $k_0b = 5.1$, $H_{02} = 1, \theta_2 = \pi$. The scattered radiation is also shown for $N = 3$, $H_{03} = 0.5$, $\theta_3 = 5\pi / 4$ with little changes.

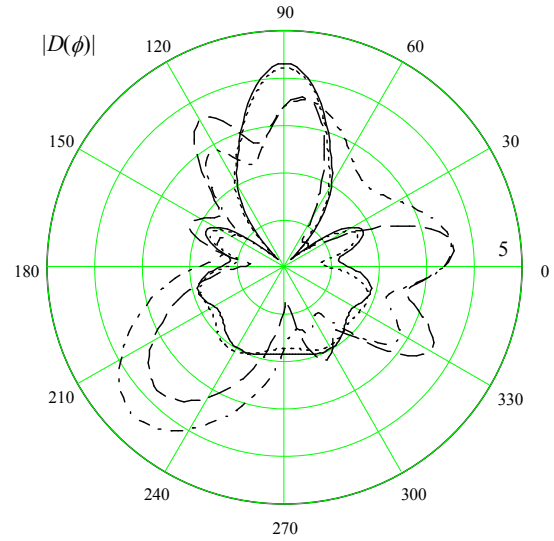


Fig. 2b. Diffracted field patterns for $k_0a = 5$, $\epsilon / \epsilon_0 = 5$, $\mu / \mu_0 = 1$, $H_{01} = 1$ and $\theta_1 = -\pi / 2$. ——— reference [11], $N=2$, $k_0b = 5.01$, $H_{02} = 0.1$, $\theta_2 = \pi$, - - - - $N=2$, $k_0b = 5.1$, $H_{02} = 1$, $\theta_2 = \pi$, - · - · - $N=3$, $k_0b = 5.1$, $H_{02} = H_{03} = 1$, $\theta_2 = \pi$, $\theta_3 = 5\pi / 4$.

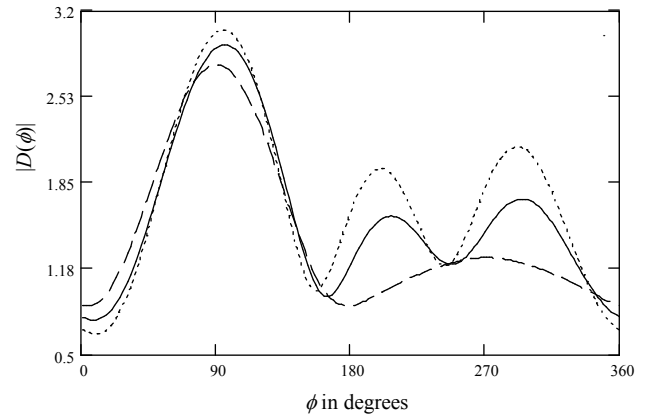


Fig. 3a. Diffracted fields for $N = 3$, $k_0a = 1$, $k_0b = 1.4$, $H_{01} = H_{02} = H_{03} = 1$, $\epsilon / \epsilon_0 = 5$, $\mu / \mu_0 = 1$, $\theta_1 = 0$ and $\theta_2 = \pi$. ——— $\theta_3 = \pi / 3$, $\theta_3 = \pi / 4$, - - - - $\theta_3 = \pi / 2$.

Possible variations of the diffracted field with respect to θ_l are illustrated in Figure 3. The far diffracted field patterns are plotted in Figure 3a for $N = 3$, $k_0a = 1$, $k_0b = 1.4$, $H_{01} = H_{02} = H_{03} = 1$, $\epsilon / \epsilon_0 = 5$, $\mu / \mu_0 = 1$ and $\theta_1 = 0$, $\theta_2 = \pi$ and $\theta_3 = \pi / 3, \pi / 4$ and $\pi / 2$. For this coating thickness the patterns are simple and the main lobe is around $\phi = 90$ degrees. Side lobes also exist but very low for $\theta_3 = \pi / 2$. Also, Figure 3b shows the diffracted patterns for the same values except that $\epsilon / \epsilon_0 = 1$ and $\mu / \mu_0 = 5$. We can

notice that the main lobe is around $\phi = 180$ degrees but with more side lobes for all values of θ_L .

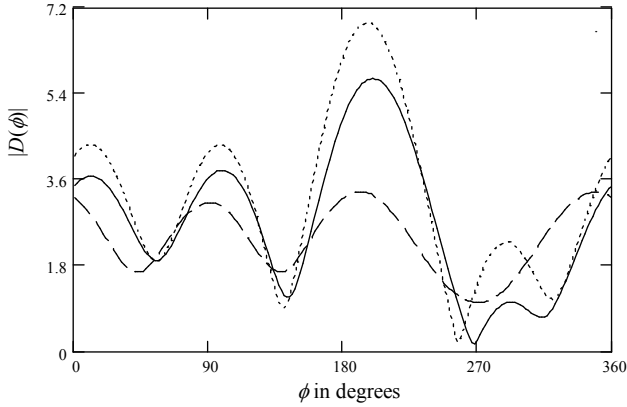


Fig. 3b. Diffracted fields for $N = 3, k_0a = 1, k_0b = 1.4, H_{01} = H_{02} = H_{03} = 1, \epsilon / \epsilon_0 = 1, \mu / \mu_0 = 5, \theta_1 = 0$ and $\theta_2 = \pi$.
 ——— $\theta_3 = \pi / 3$, $\theta_3 = \pi / 4$, - - - - $\theta_3 = \pi / 2$.

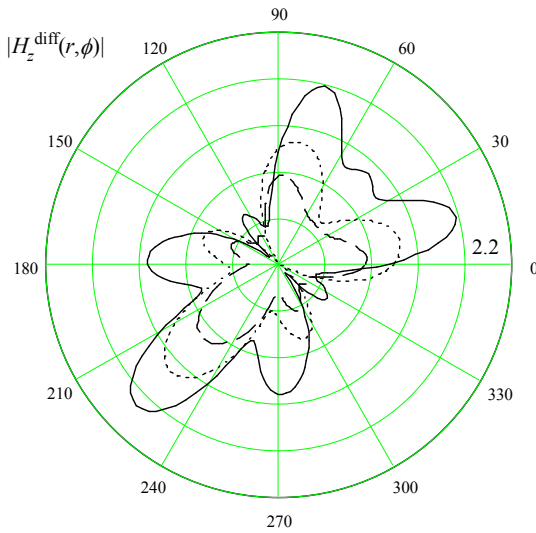


Fig. 4a. Diffracted fields for $N = 3, k_0a = 5, k_0b = 5.1, H_{01} = H_{02} = 1, H_{03} = 0.5, \epsilon / \epsilon_0 = 5, \mu / \mu_0 = 1, \theta_1 = -\pi / 2, \theta_2 = \pi$ and $\theta_3 = 5\pi / 4$.
 ——— $k_0r = 5.1$, $k_0r = 8$, - - - - $k_0r = 15$.

The diffracted field patterns can also be plotted from equation 4 directly without the large r asymptotic approximation of the Hankel function as in equation 21. The results in this case show the field close to the structure for values of $r \geq b$ in free space. Figure 4a shows the diffracted field for Diffracted field patterns for $N = 3, k_0a = 5, k_0b = 5.1, H_{01} = H_{02} = 1, H_{03} = 0.5, \epsilon / \epsilon_0 = 5, \mu / \mu_0 = 1, \theta_1 = -\pi / 2, \theta_2 = \pi, \theta_3 = 5\pi / 4, k_0r = 5.1, k_0r = 8$ and $k_0r = 15$. We can see that as r increases the pattern approaches that of the far field. In Figure 4b the diffracted field is plotted for the same values except that $\epsilon / \epsilon_0 = 1, \mu / \mu_0 = 5$

$\mu_0 = 5$ where more side lobes are generated with different amplitudes.

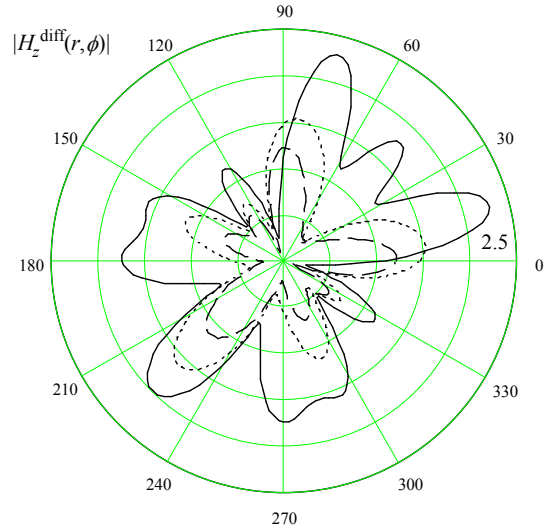


Fig. 4b. Diffracted fields for $N = 3, k_0a = 5, k_0b = 5.1, H_{01} = H_{02} = 1, H_{03} = 0.5, \epsilon / \epsilon_0 = 1, \mu / \mu_0 = 5, \theta_1 = -\pi / 2, \theta_2 = \pi$ and $\theta_3 = 5\pi / 4$.
 ——— $k_0r = 5.1$, $k_0r = 8$, - - - - $k_0r = 15$.

In Figure 5, the diffracted magnetic field in equations 4 and 21 are plotted versus k_0r in order to make a clear comparison between them. Figure 5a shows the diffracted field at $\phi = 0$ for $N = 3, k_0a = 1, k_0b = 1.4, H_{01} = H_{02} = H_{03} = 1, \epsilon / \epsilon_0 = 5, \mu / \mu_0 = 1, \theta_1 = 0, \theta_2 = \pi, \theta_3 = \pi / 3$. The curves for both equations arrive at the same numerical values as k_0r increases. This result is also reached from Figure 5b for the same parameters except $\epsilon / \epsilon_0 = 1, \mu / \mu_0 = 5$.

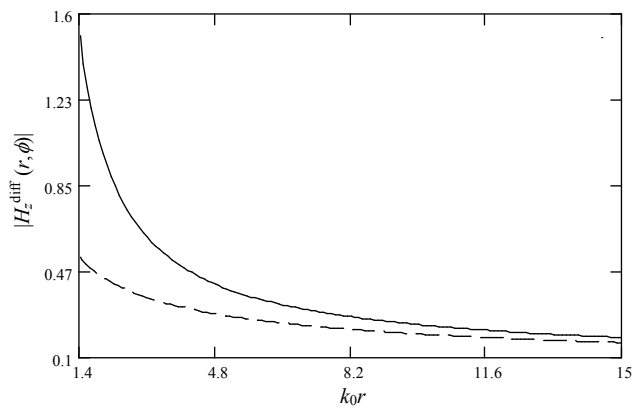


Fig. 5a. Diffracted fields at $\phi = 0$ for $N = 3, k_0a = 1, k_0b = 1.4, H_{01} = H_{02} = H_{03} = 1, \epsilon / \epsilon_0 = 5, \mu / \mu_0 = 1, \theta_1 = 0, \theta_2 = \pi$ and $\theta_3 = \pi / 3$.
 ——— Equation 4, - - - - Equation 21.

Equations 5 and 6 can also be plotted and we can verify the boundary condition in equation 11. The tangential magnetic fields in regions I and II are calculated in Figure 6 for numerical values of $r \rightarrow b^-$

in region I and $r \rightarrow b^+$ in region II. Although the tangential magnetic fields in both regions at $r = b$ are equal, we intend to find the fields very close to b to find out the accuracy of our derived expressions.

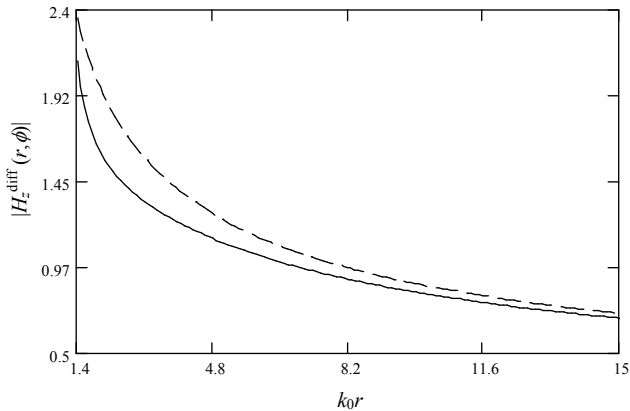


Fig. 5b. Diffracted fields at $\phi = 0$ for $N = 3$, $k_0 a = 1$, $k_0 b = 1.4$, $H_{01} = H_{02} = H_{03} = 1$, $\epsilon / \epsilon_0 = 1$, $\mu / \mu_0 = 5$, $\theta_1 = 0$, $\theta_2 = \pi$ and $\theta_3 = \pi / 3$. — Equation 4, - - - Equation 21.

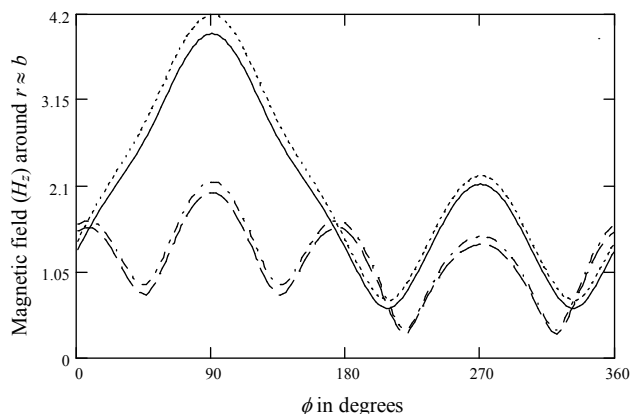


Fig. 6a. Tangential magnetic field (H_z) in regions I and II for $N = 3$, $k_0 a = 1$, $H_{01} = H_{02} = H_{03} = 1$, $\theta_1 = 0$, $\theta_2 = \pi / 2$ and $\theta_3 = \pi$. — Equation 5 for $\epsilon / \epsilon_0 = 5$, $\mu / \mu_0 = 1$, $k_0 b = 1.2$ and $k_0 r = 1.22$, Equation 6 for $\epsilon / \epsilon_0 = 5$, $\mu / \mu_0 = 1$, $k_0 b = 1.2$ and $k_0 r = 1.18$, - - - Equation 5 for $\epsilon / \epsilon_0 = 1$, $\mu / \mu_0 = 5$, $k_0 b = 1.5$ and $k_0 r = 1.52$, - · - · - Equation 6 for $\epsilon / \epsilon_0 = 1$, $\mu / \mu_0 = 5$, $k_0 b = 1.5$ and $k_0 r = 1.48$.

Figure 6a shows the tangential magnetic fields in regions I and II for $N = 3$, $k_0 a = 1$, $H_{01} = H_{02} = H_{03} = 1$, $\theta_1 = 0$, $\theta_2 = \pi / 2$ and $\theta_3 = \pi$. Equations 5 and 6 are first plotted for $\epsilon / \epsilon_0 = 5$, $\mu / \mu_0 = 1$, $k_0 b = 1.2$ and $k_0 r = 1.22$ and $k_0 r = 1.18$ respectively. We can clearly see that both curves are very similar and approach exact numerical values as $r \rightarrow b$. In addition, both equations are calculated for $\epsilon / \epsilon_0 = 1$, $\mu / \mu_0 = 5$, $k_0 b = 1.5$ and $k_0 r = 1.52$ and $k_0 r = 1.48$ respectively. We can also observe that both curves are very similar and approach exact numerical values as $r \rightarrow b$.

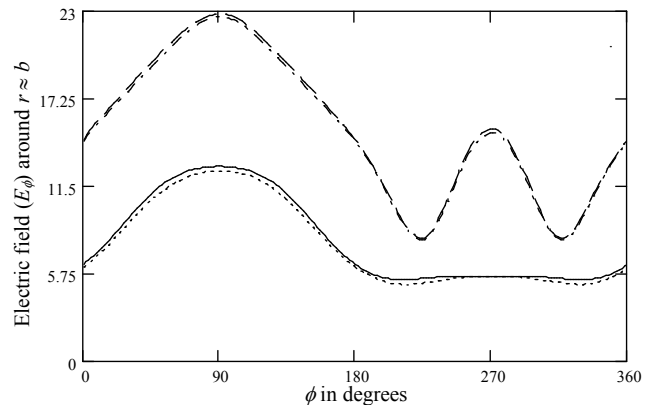


Fig. 6b. Tangential electric field (E_ϕ) in equation 8 for $N = 3$, $k_0 a = 1$, $k_0 b = 1.5$, $H_{01} = H_{02} = H_{03} = 1$, $\theta_1 = 0$, $\theta_2 = \pi / 2$ and $\theta_3 = \pi$. — Region II for $\epsilon / \epsilon_0 = 5$, $\mu / \mu_0 = 1$ and $k_0 r = 1.52$, Region I for $\epsilon / \epsilon_0 = 5$, $\mu / \mu_0 = 1$ and $k_0 r = 1.48$, - - - Region II for $\epsilon / \epsilon_0 = 1$, $\mu / \mu_0 = 5$ and $k_0 r = 1.52$, - · - · - Region I for $\epsilon / \epsilon_0 = 1$, $\mu / \mu_0 = 5$ and $k_0 r = 1.48$.

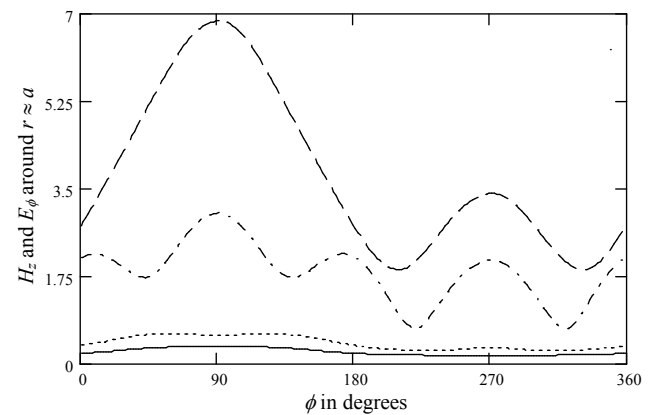


Fig. 6c. Tangential magnetic and electric fields (H_z & E_ϕ) in region I for $N = 3$, $k_0 a = 1$, $k_0 b = 1.5$, $k_0 r = 1.01$, $H_{01} = H_{02} = H_{03} = 1$, $\theta_1 = 0$, $\theta_2 = \pi / 2$ and $\theta_3 = \pi$. — Equation 9 for $\epsilon / \epsilon_0 = 5$ and $\mu / \mu_0 = 1$, Equation 9 $\epsilon / \epsilon_0 = 1$ and $\mu / \mu_0 = 5$, - - - Equation 6 for $\epsilon / \epsilon_0 = 5$ and $\mu / \mu_0 = 1$, - · - · - Equation 6 for $\epsilon / \epsilon_0 = 1$ and $\mu / \mu_0 = 5$.

The tangential electric field in equation 8 is plotted in Figure 6b in both regions for the same parameters of Figure 6a. The numerical values as $r \rightarrow b$ are very close to each other and hence all tangential fields are justified at the boundary between regions I and II. Moreover, for the same parameters except that $k_0 r = 1.01$ as $r \rightarrow a^+$ the tangential fields at the surface of the conducting circular cylinder are shown in Figure 6c as expressed in equation 6 and 9. The tangential electric field is very close to zero while there is a pattern for the tangential magnetic field, which indicates the surface current distribution on the cylinder.

The only normal field component in our study is expressed in equation 7. The coating material is assumed linear and lossless and hence there are no free charges and surface current at the interface for $r = b$. In this case the relation between the normal electric field components between regions I and II is:

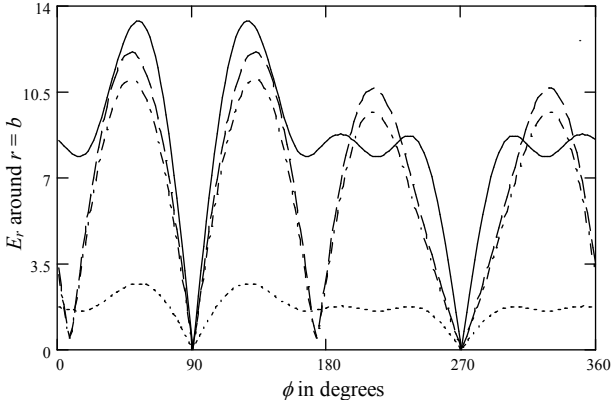
$$\epsilon E_r^I = \epsilon_0 E_r^{II} \quad (23)$$


Fig. 7a. Normal electric field (E_r) in equation 7 for $N = 3$, $k_0a = 1$, $k_0b = 1.5$, $k_0r = 1.5$, $H_{01} = H_{02} = H_{03} = 1$, $\theta_1 = 0$, $\theta_2 = \pi/2$ and $\theta_3 = \pi$. ——— Region II for $\epsilon/\epsilon_0 = 5$ and $\mu/\mu_0 = 1$, Region I $\epsilon/\epsilon_0 = 5$ and $\mu/\mu_0 = 1$, - - - Region II for $\epsilon/\epsilon_0 = 1.1$ and $\mu/\mu_0 = 5$, - · - · - Region I for $\epsilon/\epsilon_0 = 1.1$ and $\mu/\mu_0 = 5$.

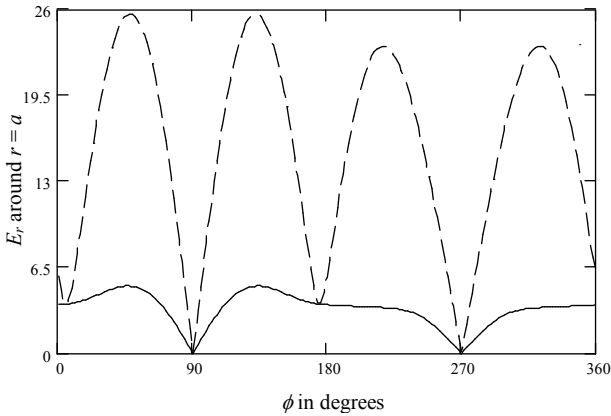


Fig. 7b. Normal electric field (E_r) in region I for $N = 3$, $k_0a = 1$, $k_0b = 1.5$, $k_0r = 1$, $H_{01} = H_{02} = H_{03} = 1$, $\theta_1 = 0$, $\theta_2 = \pi/2$ and $\theta_3 = \pi$. ——— $\epsilon/\epsilon_0 = 5$ and $\mu/\mu_0 = 1$, - - - - $\epsilon/\epsilon_0 = 1$ and $\mu/\mu_0 = 5$.

If we choose $\epsilon/\epsilon_0 = 1$, then the normal components are equal at the interface for $r = b$ between both regions. In Figure 7a, E_r is calculated in both regions for $N = 3$, $k_0a = 1$, $k_0b = 1.5$, $k_0r = 1.5$, $H_{01} = H_{02} = H_{03} = 1$, $\theta_1 = 0$, $\theta_2 = \pi/2$ and $\theta_3 = \pi$. The curves are nearly equal for $\epsilon/\epsilon_0 = 1.1$ but are far apart when $\epsilon/\epsilon_0 = 5$. In Figure 7b, the normal electric field component is also plotted on the surface of the cylinder for $r = a$ for the same parameters except that

$k_0r = 1$. The cylinder is assumed a perfect conductor and hence a surface current exists as explained previously in Figure 6c. Free surface charges (ρ_s) also exist and in this case the normal electric field component in region I is:

$$E_r^I = \frac{\rho_s}{\epsilon} \quad (24)$$

As can be seen from Figure 7b patterns are different for values of $\epsilon/\epsilon_0 = 5$ or 1.

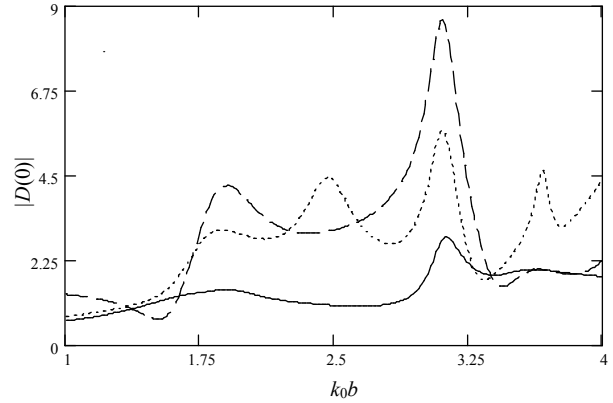


Fig. 8a. Scattered pattern at $\phi = 0$ for $N = 3$, $k_0a = 1$, $H_{01} = 1$, $\theta_1 = -\pi/2$, $\epsilon/\epsilon_0 = 5$ and $\mu/\mu_0 = 1$. ——— $H_{02} = H_{03} = 0$, $H_{02} = 1$, $\theta_2 = \pi$ and $H_{03} = 0$, - - - - $H_{02} = H_{03} = 1$, $\theta_2 = \pi$ and $\theta_3 = 0$.

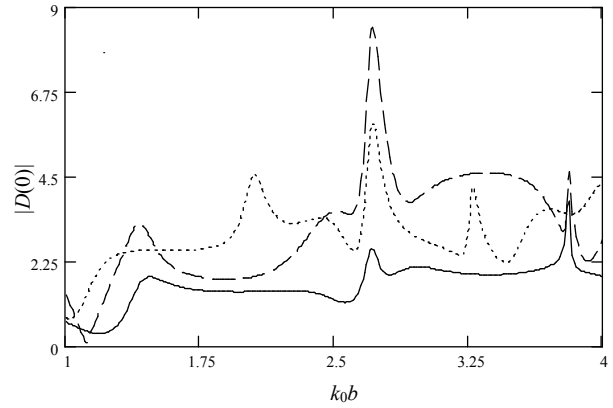


Fig. 8b. Scattered pattern at $\phi = 0$ for $N = 3$, $k_0a = 1$, $H_{01} = 1$, $\theta_1 = -\pi/2$, $\epsilon/\epsilon_0 = 1$ and $\mu/\mu_0 = 5$. ——— $H_{02} = H_{03} = 0$, $H_{02} = 1$, $\theta_2 = \pi$ and $H_{03} = 0$, - - - - $H_{02} = H_{03} = 1$, $\theta_2 = \pi$ and $\theta_3 = 0$.

Finally, the diffracted fields can be calculated with respect to the coating thickness to locate peak values as in Figure 8. The pattern at $\phi = 0$ is shown in Figure 8a for $N = 3$, $k_0a = 1$, $\epsilon/\epsilon_0 = 5$, $\mu/\mu_0 = 1$, $H_{01} = 1$, $\theta_1 = -\pi/2$ for one, two and three incident waves respectively. In addition, in Figure 8b, patterns are calculated for the same parameters except that $\epsilon/\epsilon_0 = 1$, $\mu/\mu_0 = 5$ and in both cases we can notice higher peaks as N increases.

4 Conclusion

The TE scattered field patterns were found for the problem of N incident plane waves on a circular cylinder covered by a coating material. The solution explained several field characteristics and the influence of other incident waves to the diffracted fields. Normal and tangential components of the magnetic and electrical fields were examined. The results indicate that additional incident waves can cause various changes in the diffracted far fields for different parameters. In addition, the coating thickness can influence the field patterns and magnitude. The approximate asymptotic expressions for the fields were also examined at a far point. Moreover, tangential components for the magnetic and the electrical fields were investigated at the boundaries and showed acceptable results.

References

- [1] Tan, C., "Backscattering from a Dielectric-Coated Infinite Cylindrical Obstacles", *Journal of Applied Physics*, Vol. 28, No. 5, pp. 628–633, May 1957.
- [2] Sachdeva, B. K. and Hurd, R. A., "Scattering by a Dielectric-Loaded Trough in a Conducting Plane", *Journal of Applied Physics*, Vol. 48, No. 4, April 1977, pp. 1473–1476.
- [3] Wang, N., "Electromagnetic Scattering from a Dielectric-Coated Circular Cylinder", *IEEE Transactions on Antennas and Propagation*, Vol. 33, No. 9, September 1985, pp. 960–963.
- [4] Hinders, M. and Yaghjian, A., "Dual-Series Solution to Scattering from a Semicircular Channel in a Ground Plane", *IEEE Microwaves and Guided Waves Letters*, Vol. 1, No. 9, September 1991, pp. 239–242.
- [5] Wait, J., "Scattering of a Plane Wave from a Circular Dielectric Cylinder at Oblique Incidence", *Canadian Journal of Physics*, Vol. 33, No. 5, May 1955, pp. 189–195.
- [6] Mushref, Muhammad A., "Transverse Magnetic Scattering of Two Incident Plane Waves by a Dielectric Coated Cylindrical Reflector", *Central European Journal of Physics*, Vol. 3, No. 2, 2005, pp. 229–246.
- [7] Burghignoli, P and Cupis, P., "Plane Wave Expansion of Non-Integer Cylindrical Functions", *Optics Communications*, Vol. 199, November 2001, pp. 17–23.
- [8] Harrington, R. F., "Time-Harmonic Electromagnetic Fields", John Wiley & Sons, Inc., New York, 2001.
- [9] Stratton, J. A., "Electromagnetic Theory", McGraw-Hill, Inc., New York, 1941.
- [10] Wait, J. R., "Electromagnetic Radiation from Cylindrical Structures", Institution of Electrical Engineers, London, 1988.
- [11] Bowman, J. J., Senior, T. B. A. and Uslenghi, P. L. E., "Electromagnetic and Acoustic Scattering by Simple Shapes", Hemisphere Publishing Corporation, 1987.
- [12] Wait, J. and Mientka, W., "Slotted-Cylinder Antenna with a Dielectric Coating", *Journal of Research of the National Bureau of Standards*, Vol. 58, No. 6, June 1957, pp. 287–296.